



Studies on Parametric Optimization of HVOF-Sprayed Cr_2O_3 Coatings on Al6061 Alloy

G. S. Pradeep Kumar¹ · M. Harish Kumar¹ · Shijo Thomas¹ · H. M. Yegnesh¹ · Sharada Bharadwaj¹ · Gurumoorthy S. Hebbar¹

Received: 23 February 2021 / Accepted: 6 May 2021 / Published online: 3 June 2021
© The Indian Institute of Metals - IIM 2021

Abstract High-velocity oxy-fuel (HVOF) is a widely used thermal spray technique to obtain high density, high bond strength, and improved hardness coatings. In the present work, optimization of HVOF process parameters was carried out using the Taguchi method to minimize porosity and improve microhardness, and bond strength of Cr_2O_3 coatings. Based on the signal-to-noise ratio and analysis of variance, the significance of each process parameter and optimum parameter combination is obtained. Based on the signal-to-noise ratio, the most significant process parameter affecting porosity and microhardness was standoff distance, while for bond strength, it was powder feed rate. An optimal combination of process parameters for porosity, microhardness, and bond strength was obtained from S/N ratio analysis. For porosity, optimal parameters were standoff distance of 100 rpm, powder feed rate of 30 g/min, and gun speed of 250 mm/s. The optimal process parameters for microhardness were standoff distance of 300 rpm, powder feed rate of 50 g/min, and gun speed of 200 mm/s. Finally, for bond strength, the optimal process parameters were standoff distance of 300 rpm, powder feed rate of 50 g/min, and gun speed of 250 mm/s. Statistical results for porosity, microhardness, and bond strength showed that the difference between the predicted R^2 and adjusted R^2 values were relatively minimal and close to the one highlighting the fitness of the regression model employed for analysis. Fracture analysis after bond

strength test showed combined adhesion/cohesion type failure for the Cr_2O_3 coatings.

Keywords Chromium oxide coating · Taguchi method · Porosity · Microhardness · Adhesion

1 Introduction

Surface coatings developed using thermal spray techniques have emerged as prominent solutions for protecting engineering structures or components against degradation processes like wear, erosion, abrasion, and corrosion. The main intention behind the development of the surface coatings was to address the serious economic loss and reduced design life of engineering structures or components by the degradation processes. The global business of thermal spray technology is expected to witness exponential growth and is expected to reach USD 17.63 billion by 2027. At the present surface, coatings are not limited to thermal barrier applications for gas turbine but also been used in other industries like dentistry, biomedical, construction, energy, and sports. Based on the requirement of applications, appropriate coating based on pure metals, carbides, oxides, cermet, and fused self-fluxing alloys is applied using a suitable spray technique [1–5].

Out of all available spraying techniques, the high-velocity oxy-fuel (HVOF) process has special significance. The surface coatings developed using HVOF are known to have the same composition as spraying powder and low porosity content than plasma spray coatings [6–8].

Other benefits of HVOF include high density, high bond strength, better surface finish, improved toughness, and hardness. As of now, HVOF is used to coat tungsten carbide, chromium carbide, high entropy alloys, nickel-based,

✉ G. S. Pradeep Kumar
pradeepkumar.gs@christuniversity.in

¹ Department of Mechanical and Automobile Engineering,
CHRIST (Deemed To Be University), Bangalore 560074,
India

and Fe-based coatings [9–13]. For instance, Reddy et al. [10] reported the development of Ni₃Ti and Ni₃Ti + (Cr₃C₂ + 20NiCr) coatings using HVOF technique. The porosity percentage of both the coatings was found to be in the range of $1\% < P < 2\%$. In another work, Shivalingaiah et al. [14] reported porosity analysis of Inconel 718 reinforced cubic boron nitride composite coatings. The porosity percentages for 5% to 20% cubic boron nitride reinforced composite coatings were found to be in the range of $0.98 \pm 0.22\%$ to $1.68 \pm 0.40\%$. This work shows a less than 2% porosity percentage, which implies that one can obtain dense surface coatings using HVOF.

Further, the low porosity content and high bond strength coatings in HVOF result from high kinetic energy and high impact of the powder particles. Besides, due to high velocity, the oxidation of the powder particles is significantly less, leading to dense coatings with low oxide content. On the other hand, Bolelli et al. [15] compared the microstructure and porosity content of HVOF- and APS-sprayed Cr₂O₃ coatings. The microstructure analysis showed that crack propagation through intersplat boundaries was easy in APS-sprayed Cr₂O₃ coating, while in case HVOF, the splats seemed to be well adhered with one another. The porosity analysis showed a higher porosity percentage of 6.6% for APS when compared to HVOF coating, which showed 5.5%. Undesirable operating conditions such as high temperature, corrosive environment, and frequent sliding are known to degrade components leading to catastrophic failure of the entire engineering structure. For such cases, oxide-based coatings are widely preferred to achieve the design life and improve the performance. Singh et al. [16] conducted pin-on-disk experiments as per ASTM G99-90 and found that Cr₂O₃ coating displayed lower cumulative wear rates when compared to Al₂O₃ + TiO₂ composite coating. This was attributed to the formation of the compact lubricating film due to plastic deformation of splats resulting in lower wear rate than Al₂O₃ + TiO₂ composite coating. Out of all oxides, chromium oxide (Cr₂O₃) possesses the highest hardness, high corrosion resistance, wear-resistance, and low coefficient of friction [17, 18]. Fernandez et al. [19] reported friction and wear behavior of Cr₂O₃ coatings and counter surface AISI D2 using a block on ring tribometer. For different sliding velocities and load conditions, the Cr₂O₃ coatings showed less wear rate when compared to steel. Zamani and Valefi [20] reported the microhardness and bonding strength of Cr₂O₃, Al₂O₃/3%TiO₂, and Cr₂O₃/Al₂O₃/3%TiO₂ coatings. The Cr₂O₃ coating was found to have the highest microhardness and bonding strength of 1380 HV_{0.3} and 51 MPa compared to other coatings. Conze et al. [21] compared the microhardness and wear rate of different coatings like TiO₂, Cr₂O₃, Al₂O₃/TiO₂,

and Al₂O₃/Cr₂O₃. Out of all, Cr₂O₃ coating showed the highest hardness and lowest wear rate of ~ 1250 HV_{0.3} and $\sim 500 \times 10^{-4}$ mm³/Nm, respectively. It is seen from these works that in most of the cases, the individual Cr₂O₃ coatings show better properties than their composite or another individual ceramic counterpart. Apart from this, Cr₂O₃ and its composite coatings are also known to provide excellent resistance to elevated temperature oxidation, corrosion, and galvanic corrosion [22–25]. They can provide good resistance to the substrate against most corrosive environments and insoluble in alkalis, acids, and alcohol.

2 Experimentation

2.1 Powder and Spray Process

Cr₂O₃ powder was used as feedstock powder to coat the substrate with a size range of 5–30 μm. The SEM micrograph, EDS, and XRD of procured Cr₂O₃ powder is shown in Fig. 1a–c. The EDS spectrum of Cr₂O₃ powder showed Cr and O as main elements in the powder, and no other elements were seen indicating its high purity. The powder particles seen in the micrograph had irregular and angular morphology. The substrate selected for Cr₂O₃ coating was hot rolled Al6061 plates grit blasted with Al₂O₃ grits prior to coating. High-velocity oxy-fuel (HVOF) technique was used to coat Cr₂O₃ using Metco DJ 2600 gun (M/s Spraymet Technologies Pvt. Ltd., India). The parameters employed to achieve a coating thickness of 200 ± 20 μm are presented in Table 1. Other parameters pertaining to spraying are not mentioned in this table because they have been considered for experimental design and their effect on coating characteristics like porosity, microhardness, and bond strength are the main objectives of this study.

2.2 Design of Experiments

As mentioned earlier, the effect of three important factors, standoff distance, powder feed rate, and gun speed, was studied using Taguchi's L9 orthogonal array. The experiments were designed in 3 parameters and 3 levels as shown in Table 2. Further, the experiments were conducted as per Taguchi's L9 orthogonal array as shown in Table 3. Experimental results obtained from Taguchi method were further converted into signal to noise ratio (S/N). There are different cases here. First is the porosity percentage in the coatings. It is desirable to have minimum porosity percentage in the coatings, and for this S/N ratio criterion, 'smaller the better' was taken into consideration. To have good mechanical properties like high hardness and bonding strength, the coatings should have low porosity content. For instance, as per reference [26, 27] inverse relationship

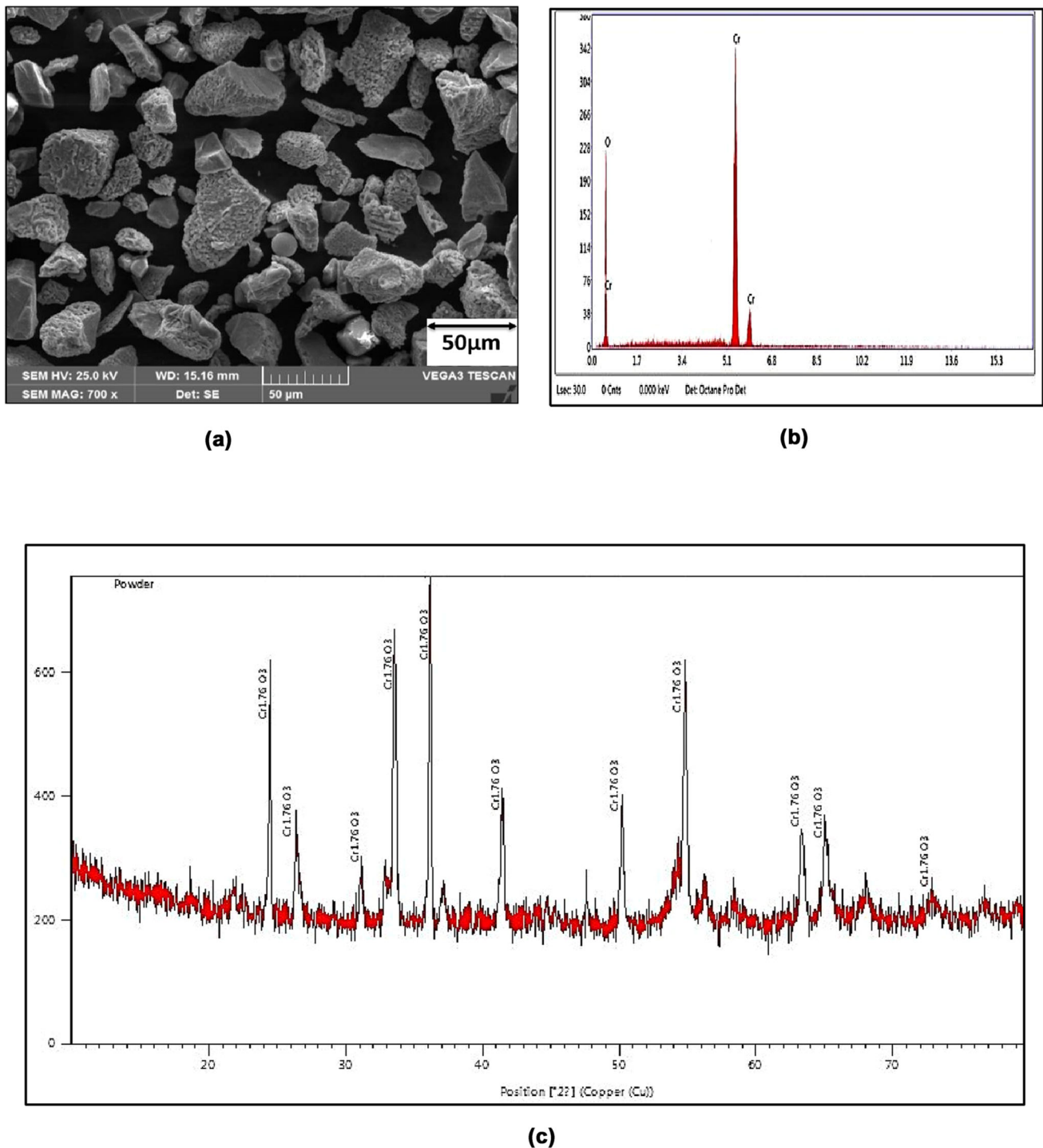


Fig. 1 a SEM and b EDS of as received Cr₂O₃ powder particles c XRD of Cr₂O₃ powder particles

exists between porosity and hardness of coatings. So in order to have maximum hardness, the coating needs to have low porosity content. As per reference [28], the corrosion resistance of coating increases as the porosity decreases. So it is desirable to have impermeable coatings to protect the underlying substrate material from the

corrosive environment. For the second and third cases, microhardness, and bond strength and S/N ratio criterion ‘larger the better’ were considered as it is desirable to have good properties. As mentioned above, the influence of each parameter on these characteristics was calculated using a statistical tool MINITAB13. Using the same tool, the

Table 1 HVOF process parameters employed for Cr₂O₃ coating

Parameter	Value
Liquid petroleum gas flow rate	1.5×10^3 m ³ /s
Air flow rate	6×10^3 m ³ /s
Oxygen flow rate	6×10^3 m ³ /s
Carrier gas flow rate	3×10^3 m ³ /s

Table 2 Levels of HVOF process parameters

Code	Parameter	Level		
		1	2	3
A	Standoff distance (mm)	100	200	300
B	Powder feed rate (g/min)	30	40	50
C	Gun speed (mm/s)	150	200	250

experimental results were subjected to analysis of variance (ANOVA) to determine each parameter's significant parameter and percentage contribution. The larger the percentage values exhibit, the stronger the influence of the parameter on the coating characteristic. The percentage contribution of each parameter less than 5% is ignored as it has no significance. Overall, three samples were tested at each combination of parameters as presented in Taguchi's L9 orthogonal array.

2.3 Testing of Coating

The Cr₂O₃ powder morphology, coating cross section analysis, and coating surface after bond strength test was studied using a scanning electron microscope (Make: Tescan Vega3). Different process parameters on

characteristics like porosity in deposited coatings, microhardness, and bond strength were studied. The porosity percentage of the developed coatings was obtained by testing as per ASTM E 2109–01 (Method A) standard. The microhardness measurements were carried out on polished coated samples as per ASTM E 92 standard. A load of 100 g for dwell time of 20 s was applied on each sample, and an average of five indentations is presented here. The bond strength test was conducted to study the bonding between Cr₂O₃ coating and Al6061 substrate. This tensile adhesion test was carried out as per ASTM C633 standard using the displacement rate of 1 mm/min [12].

3 Results and Discussion

Figure 2 shows the SEM micrograph of the cross section of the Cr₂O₃ coating on the Al6061 substrate. The Cr₂O₃ coating showed in the micrograph was obtained at a standoff distance of 200 rpm, powder feed rate of 40 g/min, and gun speed of 250 mm/s. The coating seems to be compact and dense, having good bonding with the substrate. The structure is denser near the Al6061 substrate and displays lamellar boundaries when moved toward the surface. Apart from few micro-porosities seen close to the top surface, no other defects like cracks or inter-splat boundaries are observed. Generally, poor impact velocity and temperature can result in inter-splat boundaries, which have undesirable consequences like low hardness or poor bond strength with the substrate. But in the present situation, neither inter-splat boundary nor micro-cracks emanating from such regions are seen in the SEM micrograph. The coating thickness was measured at different locations and found to have an average value of 200 ± 20 μm. The porosity, microhardness, and bond strength obtained for

Table 3 Experimental results for porosity, microhardness, and bond strength

Run	Standoff distance (mm)	Powder feed rate (g/min)	Gun speed (mm/s)	Porosity (%)	Microhardness (VHN)	Bond strength (MPa)
1	100	30	150	8.1	589.0	23.5
2	100	40	200	3.6	617.0	32.8
3	100	50	250	4.6	605.0	37.9
4	200	30	200	2.6	608.7	31.2
5	200	40	250	6.5	600.1	39.5
6	200	50	150	6.7	594.9	27.6
7	300	30	250	5.2	603.0	36.9
8	300	40	150	1.1	622.0	34.8
9	300	50	200	2.5	610.6	22.7

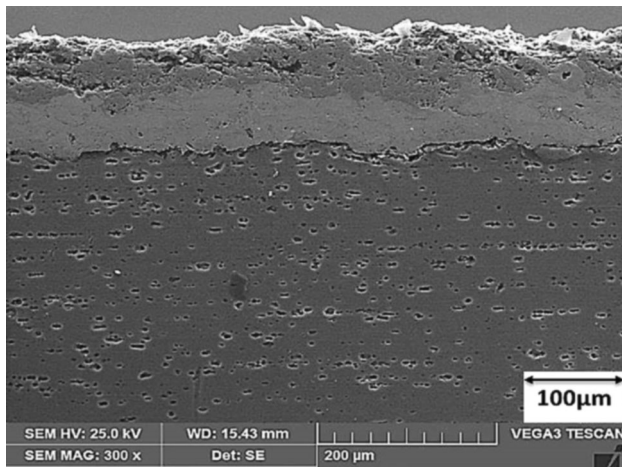


Fig. 2 Cross section micrograph of Cr₂O₃ coated Al6061 substrate

various combinations of parameters described by Taguchi’s L9 orthogonal array are presented in Table 3.

3.1 S/N Ratio Analysis

The S/N ratio is used to measure the deviation of performance characteristics from the desired value. In general, the expression for S/N ratio is given as [29, 30],

$$\eta = -10 \log(\text{mean} - \text{square deviation})$$

The mean-square deviation is different for different performance characteristics. The performance characteristic is divided into three categories, ‘smaller the better,’ ‘larger the better,’ and ‘nominal the better.’ In the present case, the important coating characteristics like porosity, microhardness, and bond strength are studied. It is understood that lower porosity in coatings is always beneficial and is desirable for a good mechanical, tribological, and corrosion point of view. Keeping this in mind, ‘smaller the better’ is more suitable for porosity, and the same has been implemented to obtain a dense coating with minimal porosity percentage. In this regard, the expression for S/N ratio is given as,

$$\eta = -10 \log \left\{ \frac{1}{n} \sum_{i=1}^n Y_i^2 \right\} \tag{1}$$

where ‘Y_i’ is the porosity value for *i*_{th} test, and n is the number of experiments. Further, the other objective of this work is to attain high microhardness and bond strength values, and for this, the performance mentioned for the above characteristic does not hold. In this regard, ‘larger the better’ characteristic is implemented for both microhardness and bond strength. The expression for S/N ratio for this characteristic is given as,

$$\eta = -10 \log \left\{ \frac{1}{n} \sum_{i=1}^n \frac{1}{Y_i^2} \right\} \tag{2}$$

Here, in this case the ‘Y_i’ corresponds to microhardness and bond strength values. From Eqs. 1 and 2, the S/N ratio for experimental results is calculated and the response table for each coating characteristics is shown in Tables 4, 5, and 6. In all the tables, the delta value and the ranking are provided for each process parameter. The delta value corresponds to a difference between the highest and lowest mean for each process parameter. A higher delta value implies a significant effect of that process parameter on corresponding coating characteristics. The S/N ratio response for porosity as shown in Table 4 shows that the standoff distance has a substantial impact while gun speed has a relatively small effect on the porosity in the coatings. This is mainly because the optimal standoff distance ensures complete melting of Cr₂O₃ particles and decreases porosity percentage. Many research works have shown that the standoff distance greatly influences the particle temperature and its in-flight velocity, which dictates the porosity and mechanical properties. Qin et al. [31] carried optimization of HVOF process parameters to obtain corrosion-resistant Fe coatings. The delta revealed that spray distance or standoff distance had most significant effect on the porosity of the coatings. It is seen that the observation made in this work supports the claim made in the present work.

Secondly, the S/N ratio response for microhardness as shown in Table 5 shows similar results as obtained in the case of porosity. One can see that there is a correlation between standoff distance, porosity, and hardness. The amount and morphology of the porosity and cracks in the coatings define the mechanical property like hardness (see Fig. 2). The complete melting of Cr₂O₃ particles result in dense coatings with minimal porosity and no visible cracks. Such coatings exhibit higher stiffness resulting in an overall increase in the microhardness [32]. However, according to Table 6, the powder feed rate has a significant effect, while standoff distance has minimal effect for good bond strength. Here, both bond strength and powder feed rate are associated with one another. Spraying any variation in the feed rate can result in poor heat transfer and the impact of powder particles result in poor splat formation and high porosity level. With the optimal powder feed rate, particles will have sufficient amount of heat energy, and complete melting can be ensured. This will help in good splat formation and reduce the amount of porosity in the coatings and improve the bond strength.

Figure 3a–c shows the main effect plots for S/N ratios for porosity, microhardness, and bond strength. As seen in Fig. 3a, the optimal process parameters to obtain minimal

Table 4 S/N ratio response for porosity

Parameter	Level			Delta	Rank
	1	2	3		
Standoff distance (mm)	– 12.93	– 16.12	– 15.19	3.19	1
Powder feed rate (g/min)	– 14.21	– 14.77	– 15.25	1.04	2
Gun speed (mm/s)	– 14.75	– 14.97	– 14.52	0.45	3

Table 5 S/N ratio response for microhardness

Parameter	Level			Delta	Rank
	1	2	3		
Standoff distance (mm)	55.69	56.11	56.41	0.72	1
Powder feed rate (g/min)	55.87	56.04	56.30	0.43	2
Gun speed (mm/s)	56.03	56.16	56.02	0.13	3

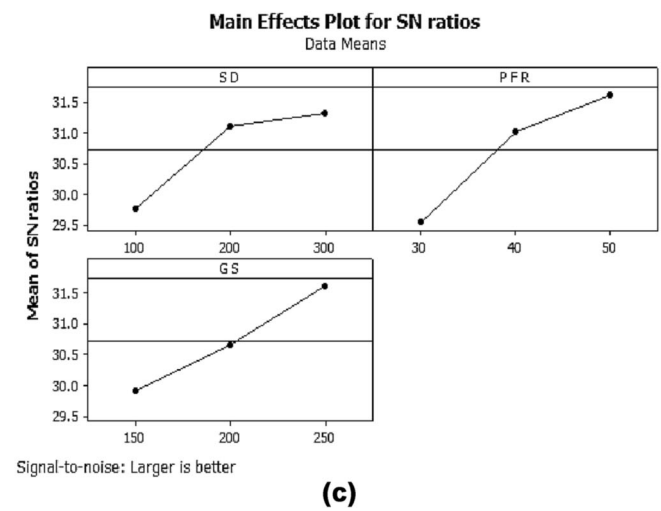
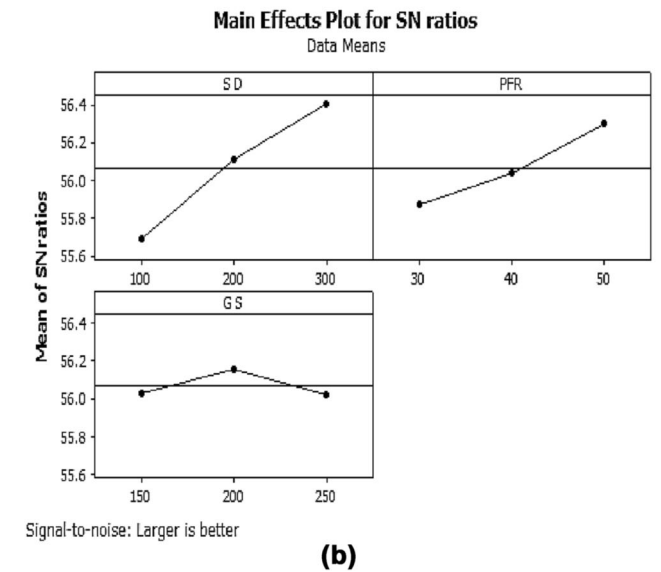
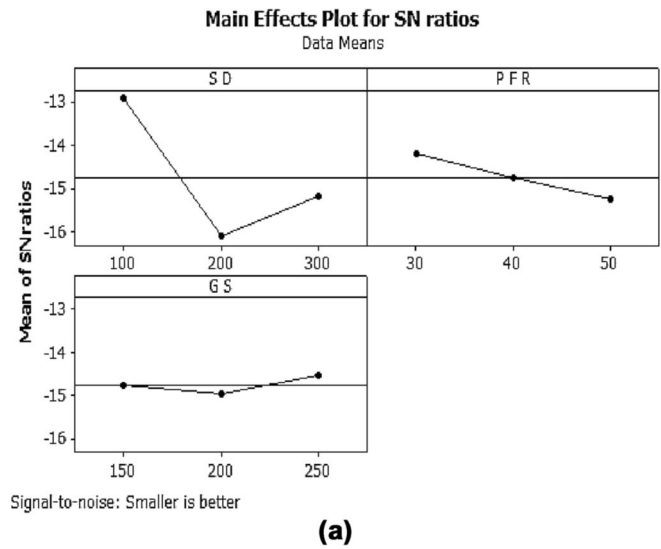
Table 6 S/N ratio response for bond strength

Parameter	Level			Delta	Rank
	1	2	3		
Standoff distance (mm)	29.77	31.11	31.31	1.54	3
Powder feed rate (g/min)	29.55	31.03	31.61	2.06	1
Gun speed (mm/s)	29.92	30.65	31.62	1.70	2

porosity are standoff distance of 100 rpm, powder feed rate of 30 g/min, and gun speed of 250 mm/s. During the spray process, the increase in standoff distance can cause a drop in temperature of droplets and cause re-solidification. In addition to this, the in-flight velocity of molten droplets drops, leading to poor splat-to-splat bonding. The decrease in temperature and low impact velocity causes a considerable amount of porosity in the coatings. This is why a smaller value of standoff distance is suggested to obtain a minimal porosity level. The optimal process parameters to obtain high microhardness are standoff distance of 300 rpm, powder feed rate of 50 g/min, and gun speed of 200 mm/s (see Fig. 3b). The higher the powder content, the better is the compactness and dense is the coating. A lower powder feed rate requires a higher number of passes to attain the required coating thickness. The chances of flying off smaller particles are very high due to which porosity is formed in coatings, causing a drop in the microhardness value. Finally, for better bond strength, the optimal combination of process parameters as seen in Fig. 3c is a standoff distance of 300 rpm, a powder feed rate of 50 g/

min, and a gun speed of 250 mm/s. It is seen that with the increase in standoff distance and powder feed rate, the bond strength of coatings is increasing. The higher feed rate ensures that small powder particles do not fly off from their path and are deposited on the substrate. The splats of Cr_2O_3 are densely deposited with minimal porosity leading to good adhesion strength with the Al6061 substrate. It is well known that the adhesion strength is usually restricted to bonding between the coating and substrate. One can achieve high adhesion strength using HVOF technique to produce high bond strengths due to the energy released from high-velocity impacts. However, if defects like pores and cracks are formed at the interface, adhesion between the coating and substrate will be insufficient and ineffective as they are primary nucleation sites of failure. Many research works have reported that the increase in porosity can significantly drop in microhardness, adhesive, and deposited coatings' cohesive strength [33, 34]. If the porosity is low, then the possibility of coating adhesion with the substrate will be good.

Fig. 3 Main effect plots for S/N ratios for **a** porosity, **b** microhardness, and **c** bond strength



Further, the smaller standoff distance results in defects like splat boundaries, un-melted particles, and pores. This is mainly because the Cr_2O_3 particles tend to stay in the flame at shorter periods due to which they might not achieve the required temperature to melt or sufficient inflight velocity to reach the substrate to have good bonding [35]. In order to have high adhesion strength, higher standoff distance is recommended as optimal process parameter. The observation made here is in line with the work reported by Praveen et al. [36] on the optimization of process parameters using Taguchi technique. The HVOF-sprayed NiCrSiB/WC–Co coatings showed better erosion resistance when the standoff distance of 300 mm was maintained. This has been attributed to the fact that at this standoff distance, the higher temperature and velocity are imposed on the powder particles which help in deposition of dense and compact coatings. Further, the response graphs for porosity, microhardness, and bond strength are shown in Fig. 4a–c. The three-dimensional graphs are plotted against the process parameters to evaluate their influence on the three coating characteristics. The valley represents minimum influence, while the peak represents maximum influence [37]. As shown in Fig. 4a, the higher and lower levels of standoff distance resulted in lower porosity, while the intermediate level or peak as shown in the contour graph gives the higher porosity in the deposited coatings. In the case of microhardness, as shown in Fig. 4b, the contour graph shows an increase in peak level with an increase in standoff distance and powder feed rate. This indicates that an increase in both the process parameters helps in a greater amount of Cr_2O_3 particles to impact the surface at higher velocities resulting in compact and dense coatings, which causes microhardness to increase. Finally, the bond strength increases and reaches the apex with increased gun speed (Fig. 4c). On the other hand, at a higher level of standoff distance, the response of the plot reaches a trough indicating a decrease in coating bond strength.

3.2 ANOVA Analysis

ANOVA analysis is another important step to investigate the most important process parameter, which greatly influences the porosity, microhardness, and bond strength. In ANOVA analysis, the most important factor is the Fisher's value (F) which is calculated for all process parameters. The ratio of mean square of process parameter to the mean square of the error is given by the ratio of mean square of process parameter. If the F value is less than 0.05, such parameters are considered insignificant and ignored. Tables 7, 8, and 9 outline the ANOVA results for porosity, microhardness, and bond strength for Cr_2O_3 coatings. For porosity and microhardness, as seen in Tables 7 and 8, the

F value for the standoff distance is higher than other parameters and has significant influence while gun speed has least. However, for bond strength, the most significant factor is powder feed rate, while standoff distance has the least effect. Further, Table 10 shows the statistical results for porosity, microhardness, and bond strength. In general, the R^2 value is expected to be near, which means the deviation between experimental and expected should be as low as possible [31].

For porosity, the predicted R^2 value is 99.69%, while adjusted R^2 value is 98.76%. Similarly, predicted R^2 and adjusted R^2 values for microhardness are 98.51% and 94.02%, respectively. The difference between both the values is quite minimal and close to one. The porosity and microhardness the predicted R^2 values are in good agreement with the adjusted R^2 values. On the other hand, the predicted R^2 and adjusted R^2 values for bond strength are 95.58% and 82.31%, respectively. The adjusted R^2 value is 82.31% and the regression model could not explain the remaining 17.69% deviation. Though the deviation is large compared with porosity or microhardness, the adjusted R^2 value for bond strength is close to one that highlights the fitness of this model. This highlights that the developed empirical relationships are correct and can be used to predict the porosity and microhardness of the Cr_2O_3 coatings. This goodness of fit can also be employed to predict the coating microhardness for a given value of porosity.

3.3 Post-Adhesion Test Analysis

After bond test, the fractured surfaces are subjected to microscopic analysis to study the mode of failure and correlate with the process parameters. The SEM micrographs of Cr_2O_3 coatings after bond strength test are shown in Fig. 5a–d. As seen in the micrographs, all the coatings display combined adhesion/cohesion type failure or mixed type of failure is when failure initiates with the adhesive failure followed by coating fracture. This type of failure is clearly depicted in Fig. 6, where the failure starts with adhesive failure followed by cohesive failure especially at the interface between lamellas and partially or unmelted particles. In the case of coating 1 as shown in Fig. 5a, the failure is a combination of adhesion/cohesion type. Complete failure is not observed, and the amount of coating remnants on the substrate surface is quite nominal. On the other hand, the main mode of failure for coating 6 is same as that of coating 1 with some traces of coating remnant found on the substrate surface (see Fig. 5b). The main difference between coatings 1 and 6 is that, the surface area covered by the coating remnants is quite large for coating 6. However, when coating 7 is considered, the coating covers larger surface of the substrate surface (see Fig. 5c). Compared to other coatings, the fraction of coating

Fig. 4 Response graphs for **a** porosity, **b** microhardness, and **c** bond strength

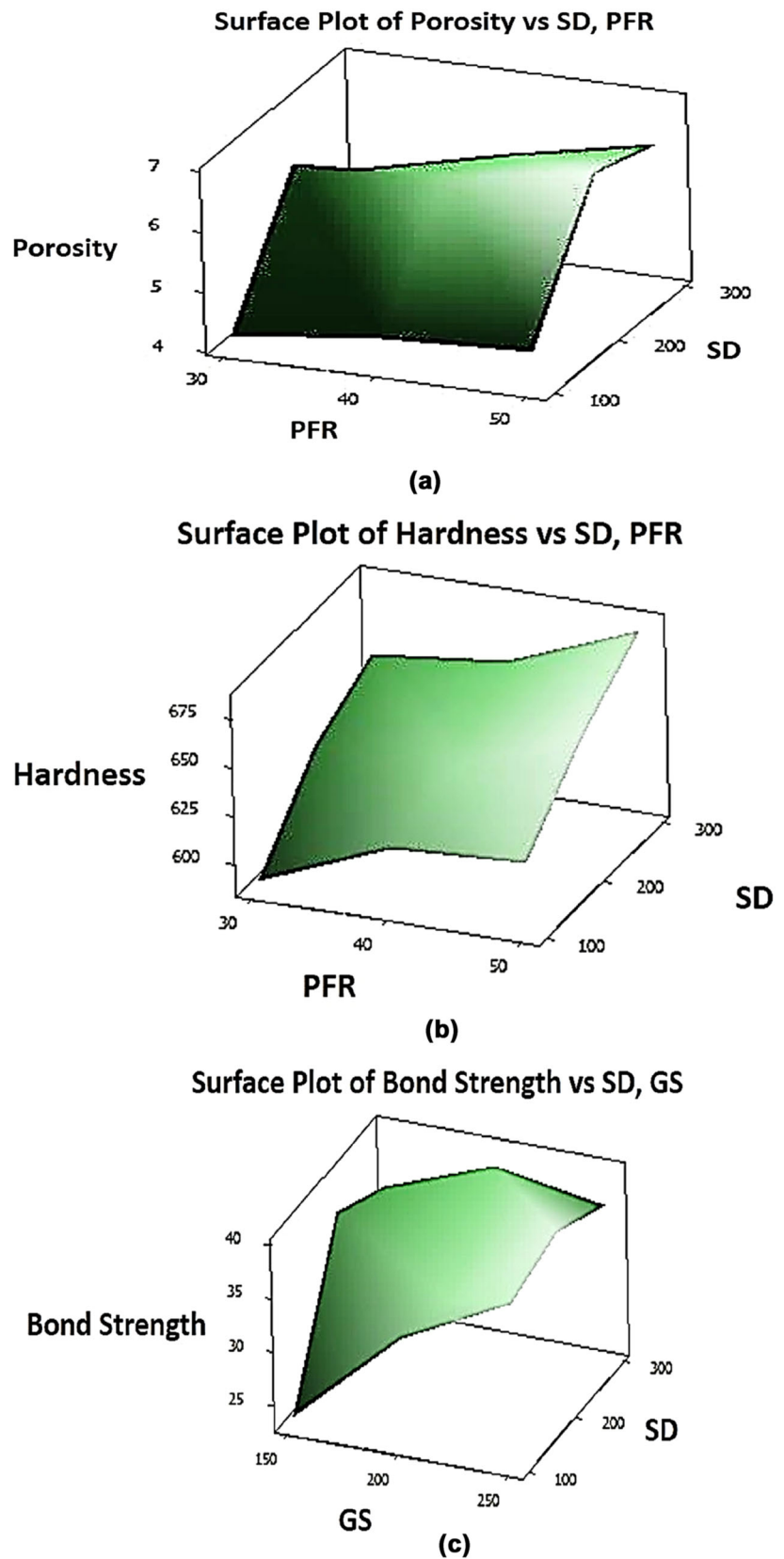


Table 7 ANOVA results for porosity

Source	DF	Seq SS	Adj SS	Adj MS	<i>F</i>	<i>P</i>
S D	2	16.1632	16.1632	8.0816	287.9	0.003
P F R	2	1.6367	1.6367	0.8183	29.15	0.033
G S	2	0.298	0.298	0.149	5.31	0.159
Error	2	0.0561	0.0561	0.0281		
Total	8	18.1541				

Table 8 ANOVA results for microhardness

Source	DF	Seq SS	Adj SS	Adj MS	<i>F</i>	<i>P</i>
S D	2	0.77678	0.77678	0.38839	47.00	0.021
PFR	2	0.27755	0.27755	0.13878	16.79	0.056
G S	2	0.0348	0.0348	0.0174	2.11	0.322
Error	2	0.01653	0.01653	0.00826		
Total	8	1.10567				

Table 9 ANOVA results for bond strength

Source	DF	Seq SS	Adj SS	Adj MS	<i>F</i>	<i>P</i>
S D	2	4.1913	4.1913	2.0957	5.92	0.145
P F R	2	6.7782	6.7782	3.3891	9.57	0.095
G S	2	4.3422	4.3422	2.1711	6.13	0.14
Error	2	0.7085	0.7085	0.3543		
Total	8	16.0203				

Table 10 Statistical results for coating characteristics

Response	<i>R</i> -squared	Adjusted <i>R</i> -squared
Porosity	99.69%	98.76%
Microhardness	98.51%	94.02%
Bond strength	95.58%	82.31%

remnants on the substrate surface of coating 9 is quite smaller as seen in Fig. 5d. The small size patches of coating are found to be scattered all over the substrate surface.

As observed, all the coatings depict mixed-mode failure and such failures usually start with adhesive failure followed by separation via epoxy. Though the coating failure initiates at the coating/substrate interface, it proceeds through the different locations like the interface between the lamellas and other interfaces between lamellas and un-

melted particles. If the bonding between the lamellas is not good or the amount of un-melted particles is higher in the coating, there are high chances of low bond strength. As seen in the SEM micrographs, the coatings are removed in small size patches which means that the cracks extend from the coating/substrate interface to the weak interfaces of lamella/un-melted particles. The lamella and un-melted particles generally have weak cohesion between them and can cause local fracture with increased strain. This is quite well reflected in the SEM micrograph where the substrate of coatings 1 and 6 show minimal coating remnant, while in case of coating 7, coating covers larger surface. Further, this claim is well supported by the bond strength values as shown in Table 3. The bond strength of coatings 1, 6, 7, and 9 is 23.5 MPa, 27.6 MPa, 36.9, and 22.7 MPa. One can see that the coating 7 which shows larger coating remnant showing higher bond strength value [38]. Further, to have a clear picture of coating failure initiation at coating/surface interface, photographs of the entire

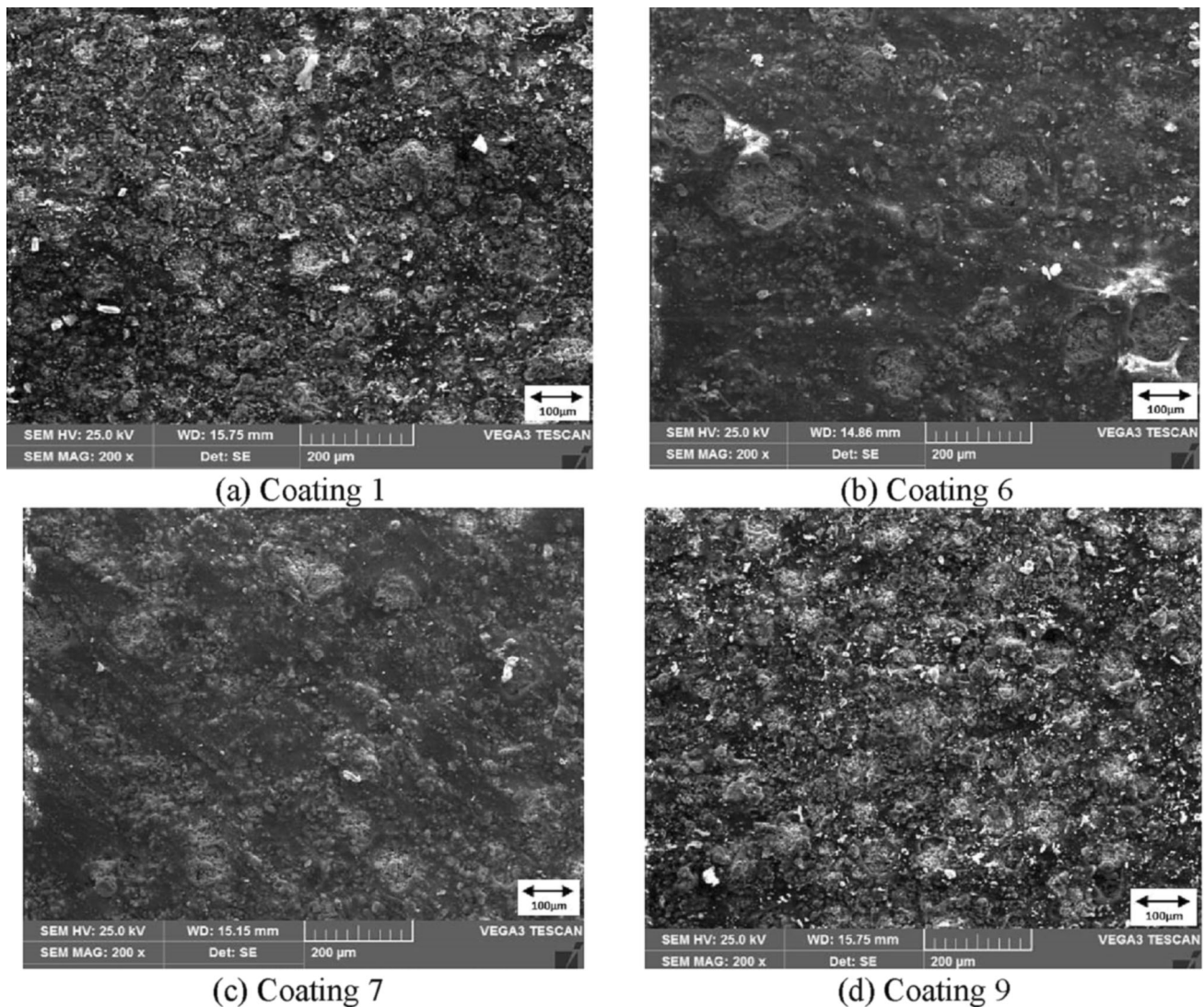


Fig. 5 Fracture surface of Cr_2O_3 coatings at standoff distance (mm), powder feed rate (g/min) and gun speed (mm/s) of **a** 100, 30, 150; **b** 200, 50, 150; **c** 300, 30, 250, and **d** 300, 50, 200

fractured surface have been taken. Figure 6a, b shows the photographs of coatings 7 and 9 taken after bond test. The failure initiation at the interface is highlighted in the checked yellow box for the two coatings.

The higher bond strength between the Cr_2O_3 coating and the Al6061 substrate is due to multiple reasons: metallurgical bonding, mechanical locking, and gun speed [39]. High impact velocity along with completely melted Cr_2O_3 particles promotes localized melting of the substrate surface. In addition to this initial grit blasting, when particles with high kinetic energy are propelled at the substrate surface, it could increase in interface temperature due to conversion of particle kinetic energy into heat energy due to impact with the substrate. Such interactions could lead to the ejection of molten material from both substrate and particles (coating) side. When the localized melting of the

substrate occurs, it triggers good metallurgical bonding between the splats and substrate surface. In such a scenario, there is fresh metal to metal contact resulting in new microstructure. This leads to improvement in the micro-hardness and bond strength of the coatings [40]. Besides, use of Al_2O_3 particles help in the formation of optimal surface roughness. This surface roughness helps in the mechanical anchoring of splats onto the substrate surface. Further, gun speed also plays an important role and as mentioned in previously published literature, the adhesion strength increases with the increase in gun speed [41]. In this case, the spraying process was carried out at the maximum gun speed of 250 mm/s and could be one of the prominent reasons for the high adhesion strength value.

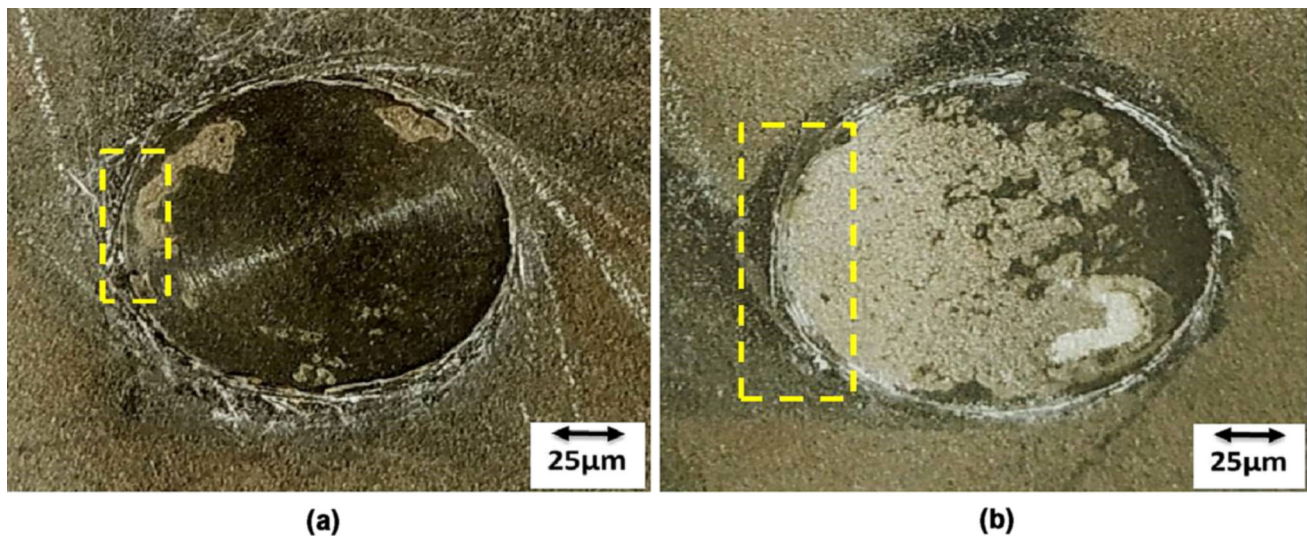


Fig. 6 Photographs of fractured surface Cr_2O_3 coatings at standoff distance (mm), powder feed rate (g/min) and gun speed (mm/s) of **a** 300, 30, 250 and **b** 300, 50, 200

4 Conclusions

The effect of spray process parameters like standoff distance, powder feed rate, and gun speed on porosity, microhardness, and bond strength was studied using Taguchi's L9 orthogonal array to obtain dense, compact, and good mechanical properties based Cr_2O_3 coating. The conclusions drawn from this work are as follows,

- Based on the delta value obtained from S/N ratio and ANOVA analysis, the standoff distance was a significant process parameter for porosity and microhardness, while for bond strength, it was powder feed rate.
- The optimal values for process parameters like standoff distance, powder feed rate, and gun speed to obtain minimal porosity were 100 rpm, 30 g/min, and 250 mm/s, to obtain high microhardness were 300 rpm, 50 g/min, and 200 mm/s, and finally, for better bond strength the values were 300 rpm, 50 g/min and 250 mm/s respectively.
- The difference between predicted R^2 and adjusted R^2 values for porosity and microhardness was minimal and close. Though the deviation was large for bond strength compared with porosity or microhardness, the adjusted R^2 value was close to one that highlighted the fitness of the regression model.
- The SEM analysis of fractured surfaces obtained after the bond test displayed combined adhesion/cohesion type failure for Cr_2O_3 coating.

Acknowledgements The authors wish to acknowledge their sincere thanks to the management of CHRIST (Deemed to be University), Bangalore, India, for sponsoring this research work under Minor

Research Project (Project No: MRP MNG-19). The authors would like to express their deep sense of gratitude to Dr.Iven Jose, Dean, School of Engineering and Technology, CHRIST (Deemed to be University), Bengaluru, India. The authors wish to thank Dr.R.Keshavamurthy, Professor, Department of Mechanical Engineering, Dayananda Sagar College of Engineering, Bangalore, INDIA, for his technical discussion and suggestions on preparing the manuscript.

References

- [1] Mohan S, and Mohan A, in *Anti-Abrasive Nanocoatings: Current and Future Applications*, Woodhead Publishing, (2015), p 3.
- [2] Hardwicke C U, and Lau Y, *J Therm Spray Technol* **22** (2013) 564.
- [3] Naveena B E, Keshavamurthy R, and Sekhar N, *Int J Comput Mater Sci Surf Eng* **8** (2019) 57.
- [4] Keshavamurthy R, Naveena B E, Ahamed A, Sekhar N, and Peer D, *Mater Res Express* **6** (2019) 0865i4.
- [5] Naveena B E, Keshavamurthy R, and Channabasappa B H, *Appl Mech Mater* **813** (2015) 511.
- [6] Sidhu T S, Prakash S, and Agarwal R D, *Mar Technol Soc J* **39** (2005) 53.
- [7] Keshavamurthy R, Sudhan J M, Kumar A, Ranjan V, Singh P, and Singh A, *Mater Today: Proc* **5** (2018) 24587.
- [8] Kumar G S P, Keshavamurthy R, Akhil M P, Kiran K, Thomas M J, and Hebbar GS, *Int J Mater Eng Innov* **12** (1), 1–17.
- [9] Tian Y, Zhang H, Chen X, MacDonald A, Wu S, Xiao T, and Li H, *Surf Coat Technol* **397** (2020) 126012.
- [10] Reddy N C, Kumar B S A, Ramesh M R, and Koppad P G, *Phys Met Metallogr* **119** (2018) 462.
- [11] Lobel M, Lindner T, and Lampke T, *Surf Coat Technol* **403** (2020) 126379.
- [12] Nagabhushana N, Rajanna S, Mathapati M, Ramesh M R, Koppad P G, and Reddy N C, *Mater Res Express* **6** (2019) 086451.
- [13] Milanti A, Matikainen V, Bolelli G, Koivuluoto H, Lusvarghi L, and Vuoristo P, *J Therm Spray Technol* **25** (2016) 1040.

- [14] Shivalingaiah K, Sridhar K S, Sethuram D, Murthy K V S, Koppad P G, and Ramesh C S, *Mater Res Express* **6** (2019) 126518.
- [15] Bolelli G, Lusvarghi L, Manfredini T, Pighetti Mantini F, Polini R, Turunen E, Varis T, and Hannula S-P, *Int J Surf Sci Eng* **1** (2007) 38.
- [16] Singh H, Grewal M S, Sekhon H S, and Rao R G, *Proc Inst Mech Eng Part J J Eng Tribol* **222** (2008) 601.
- [17] Pang X, Gao K, Volinsky A A, *J Mater Res* **22** (2007) 3531.
- [18] Dong S, Song B, Hansz B, Liao H, and Coddet C, *Surf Coat Technol* **225** (2013) 58.
- [19] Fernandez J E, Wang Y, Tucho R, Martin-Luengo M A, Gancedo R, and Rincon A, *Tribol Int* **29** (1996) 333.
- [20] Zamani P, and Valefi Z, *Surf Coat Technol* **316** (2017) 138.
- [21] Conze S, Grimm M, Berger L-M, Thiele S, Drehmann R, and Lampke T, *Surf Coat Technol* **405** (2021) 126702.
- [22] Reddy N C, Kumar B S A, Reddappa H N, Ramesh M R, Koppad P G, and Kord S, *J Alloys Compd* **736** (2018) 236.
- [23] Goyal K, *Tribol Mater Surf Interfaces* **12** (2018) 97.
- [24] Reddy N C, Koppad P G, Reddappa H N, Ramesh M R, Babu E R, and Varol T, *Surf Topogr: Metrol Prop* **7** (2019) 025019.
- [25] Goyal K, Singh H, and Bhati R, *Surf Eng* **36** (2020) 124.
- [26] Cho J Y, Zhang S H, Cho T Y, Yoon J H, Joo Y K, and Hur S K, *J Mater Sci* **44** (2009) 6348.
- [27] Tillmann W, Vogli E, Baumann I, Kopp G, and Weihs C, *J Therm Spray Technol* **19** (2010) 392.
- [28] Kawakita J, Kuroda S, and Kodama T, *Surf Coat Technol* **166** (2003) 17.
- [29] Puneeth N, Satheesh J, Koti V, Koppad P G, Akbarpour M R, and Naveen G J, *Mater Res Express* **6** (2019) 1065a1.
- [30] Ozel S, Vural E, and Binici M, *Fuel* **263** (2020) 116537.
- [31] Qin Y, Wu Y, Zhang J, Hong S, Guo W, Chen L, and Liu H, *J Mater Eng Perform* **24** (2015) 2637.
- [32] Gan J A, and Berndt C C, *Surf Coat Technol* **216** (2013) 127.
- [33] Tillmann W, Baumann I, Hollingsworth P, and Laemmerhirt I-A, *J Therm Spray Technol* **272** (2013) 272.
- [34] Bussmann M, Chandra S, and Mostaghimi J, Numerical Results of Off-Angle Thermal Spray Particle Impact, Thermal Spray 1999: United Thermal Spray Conference, E. Lugscheider, P.A. Kammer, Ed., Materials Park, Ohio and Dusseldorf, Germany, ASM International and DVS (1999) p 783.
- [35] Vignesh S, Shanmugam K, Balasubramanian V, and Sridhar K, *Defence Technol* **13** (2017) 101.
- [36] Praveen A S, Sarangan J, Suresh S, and Channabasappa B H, *Ceram Int* **42** (2016) 1094.
- [37] Ramachandran C S, Balasubramanian V, and Ananthapadmanabhan P V, *J Therm Spray Technol* **20** (2011) 590.
- [38] Rajesh R, and Sumathi S, *Energy Rep* **6** (2020) 1638.
- [39] Brossard S, Munroe P R, Tran A T T, and Hyland M M, *J Therm Spray Technol* **19** (2010) 1131.
- [40] Matejicek J, Vilemova M, Musalek R, Sachr P, and Hornik J, *Coatings* **3** (2013) 108.
- [41] Pulido-Gonzalez N, Garcia-Rodriguez S, Campo M, Rams J, and Torres B, *J Therm Spray Technol* **29** (2020) 384.

Publisher's Note Springer Nature remains neutral with regard to jurisdictional claims in published maps and institutional affiliations.